Available online at www.sciencedirect.com
SCIENCE DIRECT®
Journal of Sound and Vibration 269 (2004) 165–182
JOURNAL OF SOUND AND VIBRATION
www.elsevier.com/locate/jsvi

Vibration characteristics of a rotating flexible arm with ACLD treatment

E.H.K. Fung*, D.T.W. Yau

Department of Mechanical Engineering, The Hong Kong Polytechnic University, Hung Hom, Kowloon, Hong Kong, People's Republic of China

Received 20 May 2002; accepted 9 January 2003

Abstract

In this paper, the vibration behavior and control of a clamped–free rotating flexible cantilever arm with fully covered active constrained layer damping (ACLD) treatment are investigated. The arm is rotating in a horizontal plane in which the gravitational effect and rotary inertia are neglected. The stress–strain relationship for the viscoelastic material (VEM) is described by a complex shear modulus while the shear deformations in the two piezoelectric layers are neglected. Hamilton's principle in conjunction with finite element method (FEM) is used to derive the non-linear coupled differential equations of motion and the associated boundary conditions that describe the rigid hub angle rotation, the arm transverse displacement and the axial deformations of the three-layer composite. This refined model takes into account the effects of centrifugal stiffening due to the rotation of the beam and the potential energies of the VEM due to extension and bending. Active controllers are designed with PD for the piezosensor and actuator. The vibration frequencies and damping factors of the closed-loop beam/ACLD system are obtained after solving the characteristic complex eigenvalue problem numerically. The effects of different rotating speed, thickness ratio and loss factor of the VEM as well as different controller gain on the damped frequency and damping ratio are presented. The results of this study will be useful in the design of adaptive and smart structures for vibration suppression and control in rotating structures such as rotorcraft blades or robotic arms.

1. Introduction

The application of active constrained layer damping (ACLD) for vibration suppression in structures has been extensively investigated by numerous researchers. The ACLD treatment is

*Corresponding author. Tel.: +852-2766-6647; fax: +852-2365-4703.
E-mail address: mmhkfung@polyu.edu.hk (E.H.K. Fung).

0022-460X/03/$ - see front matter © 2003 Elsevier Ltd. All rights reserved.
doi:10.1016/S0022-460X(03)00046-4

usually a three-layer composite consisting of a viscoelastic damping layer sandwiched between a piezoelectric actuator layer (constraining layer) and a piezoelectric sensor layer. The treatment is bonded to the beam structure and acts as an effective smart treatment for vibration suppression and control. The viscoelastic material (VEM) properties can be measured and in general are both frequency and temperature dependent over a broad range of values [1]. There are different methods to model the VEM behavior. Some typical ones are the standard linear model [2], fractional derivatives model [3], Golla–Hughes–McTavish (GHM) model [4], anelastic displacement fields (ADF) model [5], modal strain energy (MSE) model [6], and the complex shear modulus model [7,8]. For the vibration analysis and control of beams with ACLD treatment the frequently used models are the complex shear modulus model [7–11] and the GHM model [12–14].

The beams under investigation in Refs. [10–15] are all considered to be non-rotating. The vibration of rotating beams or structures without ACLD treatment was studied extensively in Refs. [18–23]. When ACLD is applied in rotating beams or structures, the centrifugal stiffening effect due to the rotation [23] is significant. Also, the equations of motion governing the axial deformation and the chordwise bending are coupled through the gyroscopic coupling terms while the equation of motion for the flapwise bending is not coupled [19]. Modal analysis for gyroscopic systems is complex but the complex eigenvalue problem can be transformed into real one by using the method in Ref. [21]. Furthermore, if damping is included the system becomes a damped gyroscopic system with non-self-adjoint eigenvalue problem [17,22].

The vibration control of the axial deformation and the flapwise bending of rotating beam with ACLD was studied in Ref. [9]. The present paper investigates the vibration behavior and control of the axial deformation and chordwise bending of a clamped–free rotating flexible cantilever arm with fully covered ACLD treatment. The arm is rotating in a horizontal plane in which the gravitational effect and rotary inertia are neglected. The stress–strain relationship for the VEM is described by a complex shear modulus [8–11]. Hamilton's principle in conjunction with finite element method (FEM) is used to derive the governing equations of motion which takes into account the effects of centrifugal stiffening due to the rotation of the beam. PD controllers are designed for the piezosensor and actuator. The closed-loop equation of motion for the system is derived and the characteristic complex eigenvalue problem is solved numerically. The effects of different rotating speed, thickness ratio and loss factor of the VEM as well as different controller gain on the damped frequency and damping ratio are presented. The results of this study will be useful in the design of adaptive and smart structures for vibration suppression and control in rotating structures such as rotorcraft blades or robotic arms.

2. Theory and formulation

A finite element of a clamped–free flexible arm with fully covered ACLD treatment is shown in Fig. 1. The arm is of length L and is rotating in a horizontal plane at an angular velocity $\dot{\theta}$ about the clamped axis. The axial deformation and the transverse displacement (chordwise bending) of all three layers are in the plane of rotation. It is assumed that the gravitational effect and the rotary inertia are negligible. The shear deformations in the piezoelectric sensor/actuator layers and the base beam are negligible. The transverse displacement w is the same for all three layers. Linear theories of elasticity, viscoelasticity, and piezoelectricity are applicable in all three

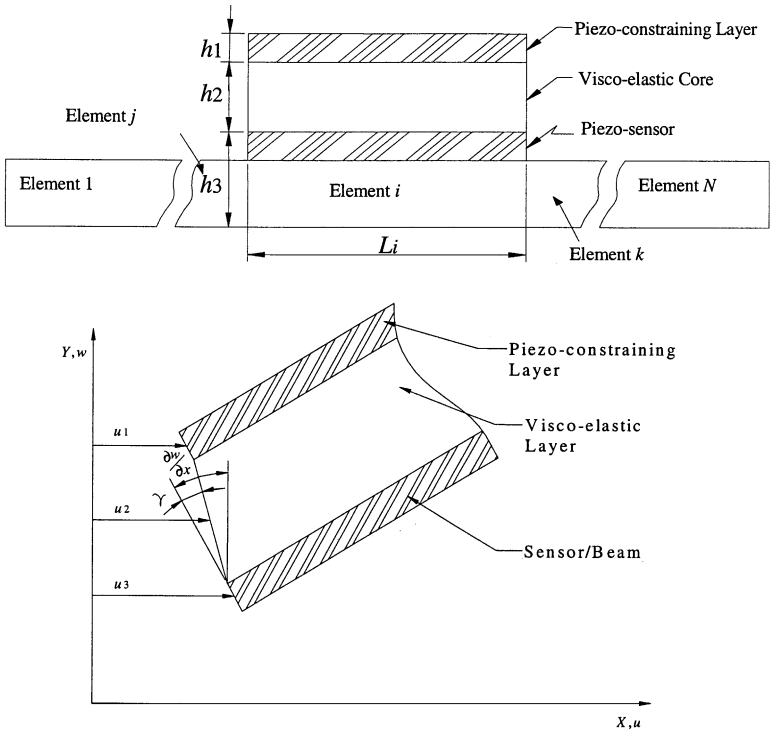

Fig. 1. A finite element of a rotating flexible arm with fully covered ACLD treatment.

layers. Also, the piezoelectric sensor and the base beam are perfectly bonded together and is considered to be reduced to a single equivalent layer. The layers are perfectly continuous and there is no slip in the interfaces. It is also assumed that thickness and density are uniform over the beam.

From the kinematic relationships between the piezoelectric (PZT) layer and the base beam the following relationship is derived:

$$u_2 = \frac{u_1 + u_3}{2} + \frac{h_1 - h_3}{4} w_x, \tag{1}$$

$$\gamma = \frac{u_1 - u_3}{h_2} + \frac{h}{h_2} w_x, \tag{2}$$

where $h = h_2 + h_1/2 + h_3/2$ and subscript x denotes partial differentiation with respect to x.

2.1. Potential energies

The potential energies associated with the extension, bending and shearing of the different layers of the beam/ACLD system are

Constraining layer:

$$\textit{extension } U_1 = \frac{1}{2} \int_0^L E_1 b h_1 u_{1x}^2 \, \mathrm{d}x, \tag{3}$$

$$bending\ U_2 = \frac{1}{2}\int_0^L E_1 I_1 w_{xx}^2\,\mathrm{d}x. \tag{4}$$

Viscoelastic layer:

$$extension\ U_3 = \frac{1}{2}\int_0^L E_2 b h_2 u_{2x}^2\,\mathrm{d}x, \tag{5}$$

$$bending\ U_4 = \frac{1}{2}\int_0^L E_2 I_2 w_{xx}^2\,\mathrm{d}x, \tag{6}$$

$$shearing\ U_5 = \frac{1}{2}\int_0^L G_2 b h_2 \gamma^2\,\mathrm{d}x, \tag{7}$$

where $G_2 = G_2'(1 + \mathrm{i}\eta)$ is the complex shear modulus of the viscoelastic material, G_2' is the storage modulus and η is the loss factor.

Sensor/beam layer:

$$extension\ U_6 = \frac{1}{2}\int_0^L E_3 b h_3 u_{3x}^2\,\mathrm{d}x, \tag{8}$$

$$bending\ U_7 = \frac{1}{2}\int_0^L E_3 I_3 w_{xx}^2\,\mathrm{d}x. \tag{9}$$

Centrifugal stiffening effect:

$$U_8 = \frac{1}{2}\int_0^L P(x,t) w_x^2\,\mathrm{d}x, \tag{10}$$

where

$$P(x,t) = \int_x^L mb\dot{\theta}^2 x\,\mathrm{d}x = \frac{1}{2} mb\dot{\theta}^2 (L^2 - x^2). \tag{11}$$

2.2. Kinetic energies

The position vector $\mathbf{r}_k$ of a spatial point in the kth layer at a distance x from the origin of the beam is given by

$$\mathbf{r}_k = (x + u_k)\mathbf{i} + w\mathbf{j}, \tag{12}$$

$$\dot{\mathbf{r}}_k = (\dot{u}_k - w\dot{\theta})\mathbf{i} + (x\dot{\theta} + u_k\dot{\theta} + \dot{w})\mathbf{j}, \tag{13}$$

where the dot denotes differentiation with respect to time t.

The total kinetic energy T of the system is

$$T = \frac{1}{2}\int_0^L \sum_{k=1}^{3} \rho_k h_k b \dot{\mathbf{r}}_k^{\mathrm{T}} \dot{\mathbf{r}}_k \,\mathrm{d}x + \frac{1}{2} J\dot{\theta}^2$$
$$= \frac{1}{2}\int_0^L \sum_{k=1}^{3} \rho_k h_k b[\dot{u}_k^2 + \dot{w}^2 + (x+u_k)^2\dot{\theta}^2 + w^2\dot{\theta}^2 + 2(x+u_k)\dot{w}\dot{\theta} - 2\dot{u}_k w\dot{\theta}]\,\mathrm{d}x + \frac{1}{2}J\dot{\theta}^2. \quad (14)$$

2.3. Work done

The work done W_1 by the external transverse loads q acting on the beam/ACLD system is given by

$$W_1 = \int_0^L qbw \,\mathrm{d}x. \quad (15)$$

The work done W_2 by the piezoelectric control forces and moments are given by

$$W_2 = \frac{1}{2}\int_0^L E_1 d_{31} b v(t) u_{1x} \,\mathrm{d}x + \frac{1}{2}\int_0^L h E_1 d_{31} b v(t) w_{xx} \,\mathrm{d}x, \quad (16)$$

where d_{31} is the piezoelectric strain constant and $v(t)$ is the piezoactuator voltage.

The work done W_3 by the applied hub torque τ is given by

$$W_3 = \tau\theta. \quad (17)$$

2.4. Equations of motion

The governing equations of motion and the boundary conditions of the beam/ACLD system are obtained by applying Hamilton's principle:

$$\int_{t_1}^{t_2} \delta\left(T - \sum_{j=1}^{8} U_j\right)\mathrm{d}t + \int_{t_1}^{t_2} \delta\left(\sum_{j=1}^{3} W_j\right)\mathrm{d}t = 0. \quad (18)$$

3. Finite element model

Let the spatial distributions of u_1, u_3 and w over any element i of the treated beam be given by

$$u_1 = a_1 x + a_2,$$
$$u_3 = a_3 x + a_4,$$
$$w = a_5 x^3 + a_6 x^2 + a_7 x + a_8, \quad (19)$$

where x is the elemental co-ordinate. The constants $\{a_1, a_2, \ldots, a_8\}$ are determined in terms of the nodal deflection vector $\mathbf{q}_i$ of the ith element which is bounded between nodes j and k. The nodal

deflection vector $\mathbf{q}_i$ is given by

$$\mathbf{q}_i = \{\, u_{1j} \quad u_{3j} \quad w_j \quad w_{jx} \quad u_{1k} \quad u_{3k} \quad w_k \quad w_{kx} \,\}^{\mathrm{T}}, \tag{20}$$

where subscript x denotes differentiation with respect to the elemental co-ordinate x.

The deflection vector $\{u_1\, u_2\, u_3\, w\, w_x\, \gamma\,\}$ is expressed in terms of the nodal deflection vector $\mathbf{q}_i$ by

$$\{\, u_1 \quad u_2 \quad u_3 \quad w \quad w_x \quad \gamma \,\}^{\mathrm{T}} = \{\, \mathbf{N}_1 \quad \mathbf{N}_2 \quad \mathbf{N}_3 \quad \mathbf{N}_4 \quad \mathbf{N}_5 \quad \mathbf{N}_6 \,\}^{\mathrm{T}} \mathbf{q}_i, \tag{21}$$

where $\mathbf{N}_1, \mathbf{N}_2, \mathbf{N}_3, \mathbf{N}_4, \mathbf{N}_5$ and $\mathbf{N}_6$ are the finite element shape functions corresponding to u_1, u_2, u_3, w, w_x and γ , respectively, and are given by

$$\begin{aligned}
&\mathbf{N}_1 = [\,1-\xi \quad 0 \quad 0 \quad 0 \quad \xi \quad 0 \quad 0 \quad 0\,],\\
&\mathbf{N}_2 = \frac{1}{2}\left(\mathbf{N}_1 + \mathbf{N}_3 + \frac{h_1 - h_3}{2}\mathbf{N}_{4x}\right),\\
&\mathbf{N}_3 = [\,0 \quad 1-\xi \quad 0 \quad 0 \quad 0 \quad \xi \quad 0 \quad 0\,],\\
&\mathbf{N}_4 = [\,0 \quad 0 \quad 1-3\xi^2+2\xi^3 \quad (\xi-2\xi^2+\xi^3)L_i \quad 0 \quad 0 \quad 3\xi^2-2\xi^3 \quad (-\xi^2+\xi^3)L_i\,],\\
&\mathbf{N}_5 = \mathbf{N}_{4x},\\
&\mathbf{N}_6 = \frac{1}{h_2}(\mathbf{N}_1 - \mathbf{N}_3 + h\mathbf{N}_{4x})
\end{aligned} \tag{22a–f}$$

and

$$\xi = \frac{x}{L_i}.$$

Defining the element coefficients and matrices as follows:

$$J_i = \int_0^{L_i} mb(x_i + x)^2 \,\mathrm{d}x, \tag{23}$$

$$\mathbf{M}_i = \int_0^{L_i} \sum_{k=1}^{3} \rho_k h_k b(\mathbf{N}_k^{\mathrm{T}}\mathbf{N}_k + \mathbf{N}_4^{\mathrm{T}}\mathbf{N}_4)\,\mathrm{d}x, \tag{24}$$

$$\mathbf{K}_i = \int_0^{L_i} \sum_{k=1}^{3} (E_k h_k b\mathbf{N}_{kx}^{\mathrm{T}}\mathbf{N}_{kx} + E_k I_k \mathbf{N}_{4xx}^{\mathrm{T}}\mathbf{N}_{4xx})\,\mathrm{d}x, \tag{25}$$

$$\mathbf{U}_{1i} = \int_0^{L_i} \sum_{k=1}^{3} \rho_k h_k b(x_i + x)\mathbf{N}_k \,\mathrm{d}x, \tag{26}$$

$$\mathbf{U}_{2i} = \int_0^{L_i} mb(x_i + x)\mathbf{N}_4 \,\mathrm{d}x, \tag{27}$$

$$\mathbf{U}_{3i} = \frac{1}{2}\int_0^{L_i} mb[L^2 - (x_i + x)^2]\mathbf{N}_{4x}^{\mathrm{T}}\mathbf{N}_{4x}\,\mathrm{d}x, \tag{28}$$

$$\mathbf{U}_{4i} = \int_0^{L_i} G_2 b h_2 \mathbf{N}_6^{\mathrm{T}}\mathbf{N}_6 \,\mathrm{d}x, \tag{29}$$

$$\mathbf{R}_i = \int_0^{L_i} \sum_{k=1}^{3} \rho_k h_k b \mathbf{N}_k^{\mathrm{T}} \mathbf{N}_4 \, \mathrm{d}x, \tag{30}$$

$$\mathbf{G}_i = \mathbf{R}_i^{\mathrm{T}} - \mathbf{R}_i, \tag{31}$$

$$\mathbf{F}_{ci} = \frac{1}{2} \int_0^{L_i} E_1 d_{31} b v(t) \mathbf{N}_{1x}^{\mathrm{T}} \, \mathrm{d}x + \frac{1}{2} \int_0^{L_i} h E_1 d_{31} b v(t) \mathbf{N}_{4xx}^{\mathrm{T}} \, \mathrm{d}x, \tag{32}$$

$$\mathbf{F}_{di} = \int_0^{L_i} q b \mathbf{N}_4^{\mathrm{T}} \, \mathrm{d}x, \tag{33}$$

where x_i is the distance from the global origin (the clamped end) to the left node of the ith element. J_i is the moment of inertia of the ith element about the clamped end. $\mathbf{M}_i$ and $\mathbf{K}_i$ are the mass and stiffness matrices, respectively. $\mathbf{U}_{3i}$ and $\mathbf{U}_{4i}$ are the matrices due to the centrifugal force and shear deformation of the VEM, respectively. The matrices $\mathbf{R}_i$ and $\mathbf{G}_i$ are due to the gyroscopic effects. The matrices $\mathbf{F}_{ci}$ and $\mathbf{F}_{di}$ represent the control force and the external load, respectively.

Substituting Eq. (21) into Eqs. (3)–(17) and Hamilton's principle (18), the equations of motion at the element level can be written in compact form as

$$\begin{bmatrix} \mathbf{M}_{\theta\theta i} & \mathbf{M}_{\theta q i} \\ \mathbf{M}_{q\theta i} & \mathbf{M}_{qqi} \end{bmatrix} \begin{Bmatrix} \ddot{\theta} \\ \ddot{\mathbf{q}}_i \end{Bmatrix} + 2\dot{\theta} \begin{bmatrix} 0 & 0 \\ 0 & \mathbf{G}_i \end{bmatrix} \begin{Bmatrix} \dot{\theta} \\ \dot{\mathbf{q}}_i \end{Bmatrix} + \begin{bmatrix} 0 & 0 \\ 0 & \mathbf{K}_{qqi} \end{bmatrix} \begin{Bmatrix} \theta \\ \mathbf{q}_i \end{Bmatrix} = \begin{bmatrix} \mathbf{Q}_{\theta i} \\ \mathbf{Q}_{qi} \end{bmatrix} + \begin{bmatrix} \mathbf{F}_{\theta i} \\ \mathbf{F}_{qi} \end{bmatrix}, \tag{34}$$

where

$$\mathbf{M}_{\theta\theta i} = J + J_i + \mathbf{q}_i^{\mathrm{T}} \mathbf{M}_i \mathbf{q}_i + 2\mathbf{U}_{1i} \mathbf{q}_i - \mathbf{q}_i^{\mathrm{T}} \mathbf{U}_{3i} \mathbf{q}_i, \tag{35}$$

$$\mathbf{M}_{\theta q i} = \mathbf{M}_{q\theta i}^{\mathrm{T}} = \mathbf{U}_{2i} + \mathbf{q}_i^{\mathrm{T}} \mathbf{G}_i, \tag{36}$$

$$\mathbf{M}_{qqi} = \mathbf{M}_i, \tag{37}$$

$$\mathbf{K}_{qqi} = \mathbf{K}_i - \dot{\theta}^2 \mathbf{M}_i + \dot{\theta}^2 \mathbf{U}_{3i} + \mathbf{U}_{4i}, \tag{38}$$

$$\mathbf{Q}_{\theta i} = -2\dot{\theta}[\mathbf{q}_i^{\mathrm{T}} \mathbf{M}_i \dot{\mathbf{q}}_i + \mathbf{U}_{1i} \dot{\mathbf{q}}_i - \mathbf{q}_i^{\mathrm{T}} \mathbf{U}_{3i} \dot{\mathbf{q}}_i], \tag{39}$$

$$\mathbf{Q}_{qi} = \dot{\theta}^2 \mathbf{U}_{1i}^{\mathrm{T}}, \tag{40}$$

$$\mathbf{F}_{\theta i} = \tau, \tag{41}$$

$$\mathbf{F}_{qi} = \mathbf{F}_{ci} + \mathbf{F}_{di} \tag{42}$$

in which $\mathbf{M}_{\theta\theta i}$ is the rotational inertia of the system, $\mathbf{M}_{qqi}$ is the generalized mass matrix, $\mathbf{M}_{\theta qi}$ is the non-linear inertia coupling between the rigid body and the elastic deformations, $\mathbf{K}_{qqi}$ is the generalized stiffness matrix and $\mathbf{G}_i$ is the gyroscopic matrix. $\mathbf{Q}_{\theta i}$ and $\mathbf{Q}_{qi}$ represent the non-linear pseudoloads. $\mathbf{F}_{\theta i}$ represents the applied hub torque and $\mathbf{F}_{qi}$ represents the summation of the control force and the external load.

Eq. (34) represents a non-linear hybrid gyroscopic dynamic system which is inertia coupled between rigid body motion and elastic deformations. Modal techniques employing mode superposition becomes inapplicable to non-linear problems [16]. For simplicity, the angular velocity $\dot{\theta}$ of the beam is assumed to be constant in this paper and also there is no external load ($\mathbf{F}_{di} = 0$). The global equation is obtained using the standard finite element assembling procedure of the elemental coefficient matrices. Linearization and assembling the elemental coefficients matrices of Eq. (34) lead to the following global equation of motion of the system:

$$\mathbf{M}_{qq}\ddot{\mathbf{q}} + 2\dot{\theta}\mathbf{G}\dot{\mathbf{q}} + \mathbf{K}_{qq}\mathbf{q} = \mathbf{F}_c, \tag{43}$$

where $\mathbf{M}_{qq}$ is real symmetric positive definite, $\mathbf{G}$ is real skew symmetric and $\mathbf{K}_{qq}$ is symmetric. $\mathbf{K}_{qq}$ is complex due to the complex shear modulus G_2 of the VEM. The matrices in Eq. (43) without the subscript i denote the global forms of the corresponding elemental coefficient matrices. The boundary conditions for Eq. (43) at the global origin (the clamped end) are zero for u_1, u_3, w and w_x.

4. Piezoelectric control forces and moments

The control force $\mathbf{F}_{ci}$ can be expressed by the piezoelectric control forces $\mathbf{F}_{pi}$ and piezoelectric moments $\mathbf{F}_{mi}$ as

$$\mathbf{F}_{ci} = \mathbf{F}_{pi} + \mathbf{F}_{mi}, \tag{44}$$

where

$$\begin{aligned}\mathbf{F}_{pi} &= \frac{1}{2}\int_0^{L_i} E_1 d_{31} b v(t) \mathbf{N}_{1x}^{\mathrm{T}}\,\mathrm{d}x \\ &= \frac{1}{2} E_1 d_{31} b v(t)[-1 \quad 0 \quad 0 \quad 0 \quad 1 \quad 0 \quad 0 \quad 0]^{\mathrm{T}},\end{aligned} \tag{45}$$

$$\begin{aligned}\mathbf{F}_{mi} &= \frac{1}{2}\int_0^{L_i} h E_1 d_{31} b v(t) \mathbf{N}_{4xx}^{\mathrm{T}}\,\mathrm{d}x \\ &= \frac{1}{2} h E_1 d_{31} b v(t)[0 \quad 0 \quad 0 \quad -1 \quad 0 \quad 0 \quad 0 \quad 1]^{\mathrm{T}}.\end{aligned} \tag{46}$$

With PD controller applied to the piezosensor voltage V_s, the voltage $v(t)$ across the piezoactuator layer is expressed as

$$v(t) = -K_p V_s - K_d \frac{\mathrm{d}V_s}{\mathrm{d}t}, \tag{47}$$

where K_p and K_d are the proportional and derivative control gains, respectively. V_s is obtained from the following formula [11]:

$$V_s = \frac{-k_{31}^2 D_d b}{g_{31} C} \sum_{i=i_s}^{i_f} \int_0^{L_i} f(x) w_{xx} \, \mathrm{d}x, \tag{48}$$

where k_{31} is the electromechanical coupling factor, D_d is the distance from the neutral axis to the sensor surface, g_{31} is the piezoelectric voltage constant and C is the capacitance of the sensor. $f(x)$ is the distribution shape function of the sensor which is extended between element i_s and i_f. For uniform sensor $f(x) = 1$. The capacitance C of the sensor is given by

$$C = 8.854 \times 10^{-12} \frac{A k_{3t}}{h_3}, \tag{49}$$

where A is the sensor surface area and k_{3t} is the dielectric constant. Substituting Eqs. (47)–(49) into Eqs. (45) and (46) gives

$$\mathbf{F}_{pi} = (K_p + K_d p)[-1 \quad 0 \quad 0 \quad 0 \quad 1 \quad 0 \quad 0 \quad 0]^{\mathrm{T}} \left[0 \quad 0 \quad 0 \quad -\frac{g}{2} \quad 0 \quad 0 \quad 0 \quad \frac{g}{2}\right] \mathbf{q}_i, \tag{50}$$

$$\mathbf{F}_{mi} = (K_p + K_d p)[0 \quad 0 \quad 0 \quad -1 \quad 0 \quad 0 \quad 0 \quad 1]^{\mathrm{T}} \left[0 \quad 0 \quad 0 \quad -\frac{gh}{2} \quad 0 \quad 0 \quad 0 \quad \frac{gh}{2}\right] \mathbf{q}_i, \tag{51}$$

where p is the $\mathrm{d}/\mathrm{d}t$ operator and g is defined by

$$g = \frac{E_1 b^2 d_{31} k_{31}^2 D_d}{g_{31} C}. \tag{52}$$

Substituting Eqs. (50) and (51) into Eq. (44) and expressing $\mathbf{F}_{ci}$ in terms of the velocity feedback gain matrix $\mathbf{G}_{vi}$ and displacement feedback gain matrix $\mathbf{G}_{pi}$ yields

$$\mathbf{F}_{ci} = -\mathbf{G}_{vi} \dot{\mathbf{q}}_i - \mathbf{G}_{pi} \mathbf{q}_i, \tag{53}$$

where

$$\begin{aligned}
\mathbf{G}_{vi} &= -K_d \mathbf{C}_1 - K_d \mathbf{C}_2, \\
\mathbf{G}_{pi} &= -K_p \mathbf{C}_1 - K_p \mathbf{C}_2, \\
\mathbf{C}_1 &= [-1 \quad 0 \quad 0 \quad 0 \quad 1 \quad 0 \quad 0 \quad 0]^{\mathrm{T}} \left[0 \quad 0 \quad 0 \quad -\frac{g}{2} \quad 0 \quad 0 \quad 0 \quad \frac{g}{2}\right], \\
\mathbf{C}_2 &= [0 \quad 0 \quad 0 \quad -1 \quad 0 \quad 0 \quad 0 \quad 1]^{\mathrm{T}} \left[0 \quad 0 \quad 0 \quad -\frac{gh}{2} \quad 0 \quad 0 \quad 0 \quad \frac{gh}{2}\right].
\end{aligned} \tag{54a–d}$$

Substituting the global form of Eq. (53) into Eq. (43), the closed-loop equation of motion for the system is

$$\mathbf{M}_{qq} \ddot{\mathbf{q}} + (2\dot{\theta}\mathbf{G} + \mathbf{G}_v)\dot{\mathbf{q}} + (\mathbf{K}_{qq} + \mathbf{G}_p)\mathbf{q} = \mathbf{0}. \tag{55}$$

The eigenvalue problem associated with Eq. (55) is second order so that it does not permit a ready solution. This difficulty can be overcome by recasting it in the state space form as

$$\mathbf{A}\dot{\mathbf{z}} + \mathbf{B}\mathbf{z} = \mathbf{0}, \tag{56}$$

where $\mathbf{z} = [\dot{\mathbf{q}}^{\mathrm{T}}\mathbf{q}^{\mathrm{T}}]^{\mathrm{T}}$ and

$$\mathbf{A} = \begin{bmatrix} \mathbf{M}_{qq} & \mathbf{0} \\ \mathbf{0} & \mathbf{I} \end{bmatrix}, \quad \mathbf{B} = \begin{bmatrix} 2\dot{\theta}\mathbf{G} + \mathbf{G}_v & \mathbf{K}_{qq} + \mathbf{G}_p \\ -\mathbf{I} & \mathbf{0} \end{bmatrix}. \tag{57}$$

The eigenvalue problem associated with Eq. (56) is

$$(\lambda_j\mathbf{A} + \mathbf{B})\mathbf{Z}_j = \mathbf{0}, \tag{58}$$

where λ_j and $\mathbf{Z}_j$ are the jth closed-loop complex eigenvalue and eigenvector, respectively. Representing the complex eigenvalue λ_j by

$$\lambda_j = \sigma_j + \mathrm{i}\omega_j, \tag{59}$$

where the real part σ_j represents the vibration exponential decay while the imaginary part ω_j is the damped frequency. The damping ratio is given by

$$\xi_j = -\frac{\sigma_j}{\sqrt{\sigma_j^2 + \omega_j^2}}. \tag{60}$$

5. Numerical simulation and results

The system is simulated using the system parameters and material properties in Table 1. The arm is divided into five finite elements. Two effective measures of the vibration characteristic of the system are the damped frequency and the damping ratio. The closed-loop eigenvalue problem

Table 1
System parameters and material properties

L	300 mm	ρ_1	$7600\,\mathrm{kg\,m^{-3}}$
L_i	60 mm	ρ_2	$1250\,\mathrm{kg\,m^{-3}}$
b	12.7 mm	ρ_3	$2700\,\mathrm{kg\,m^{-3}}$
h_1	0.762 mm	G_2'	0.2615 MPa
h_2	0.25 mm	η	0.38
h_3	2.286 mm	d_{31}	$23.0 \times 10^{-12}\,\mathrm{m\,V^{-1}}$
E_1	64.9 GPa	g_{31}	$216 \times 10^{-3}\,\mathrm{Vm\,N^{-1}}$
E_2	29.8 MPa	k_{31}	0.12
E_3	71 GPa	k_{3t}	12

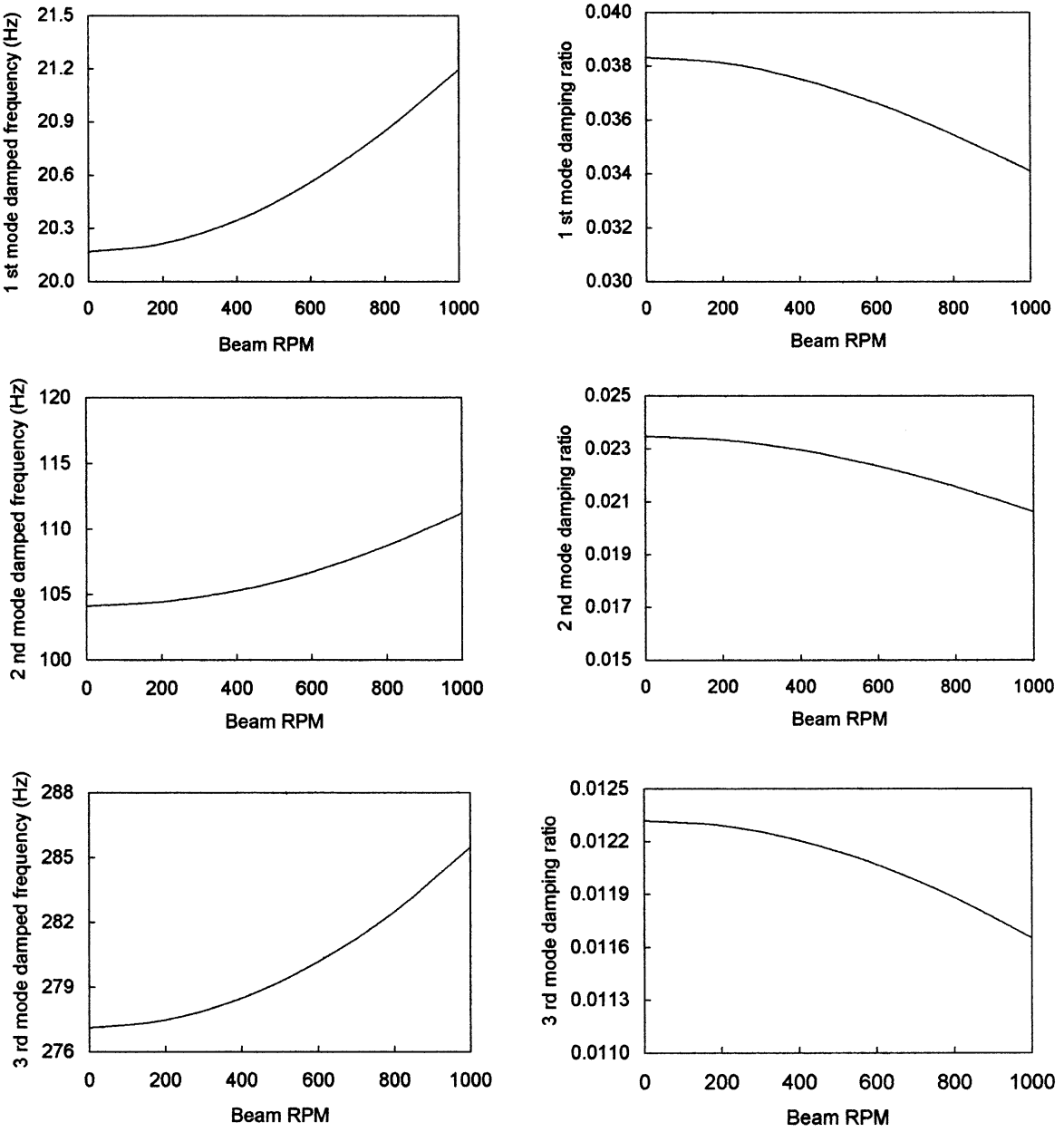

Fig. 2. The effect of angular velocity $\dot{\theta}$ on the first three modes of damped frequency and damping ratio for the case of PCLD ($K_p, K_d = 0$) when $h_2 = 0.1094h_3$ and $\eta = 0.38$.

(58) is solved numerically to obtain the damped frequency and damping ratio under different parameters of the system.

The effect of different angular velocity $\dot{\theta}$ of the arm, thickness ratio h_2/h_3 and the VEM loss factor η on the first three modes of damped frequency and damping ratio for the case of PCLD are

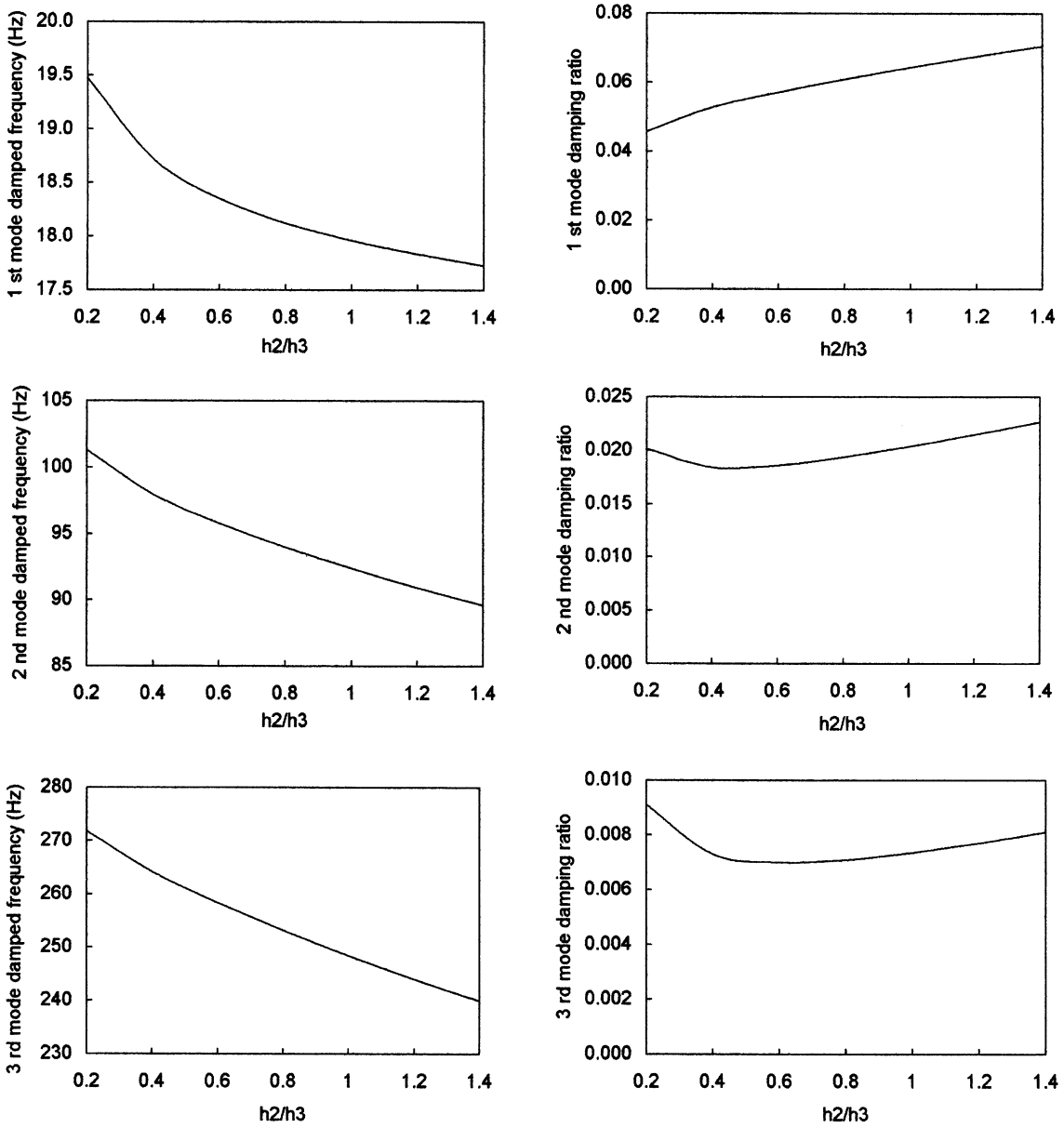

Fig. 3. The effect of thickness ratio h_2/h_3 on the first three modes of damped frequency and damping ratio for the case of PCLD ($K_p, K_d = 0$) when $\dot{\theta} = 200$ r.p.m. and $\eta = 0.38$.

shown in Figs. 2–4. PCLD (passive constrained layer damping) is the case when ACLD is unactivated such that both K_d and K_p are zero. The results shown in the figures are reasonable. It can been seen that the damped frequency increases with an increase in the rotating speed $\dot{\theta}$ while the damping ratio decreases with an increase in the rotating speed $\dot{\theta}$ which means that the

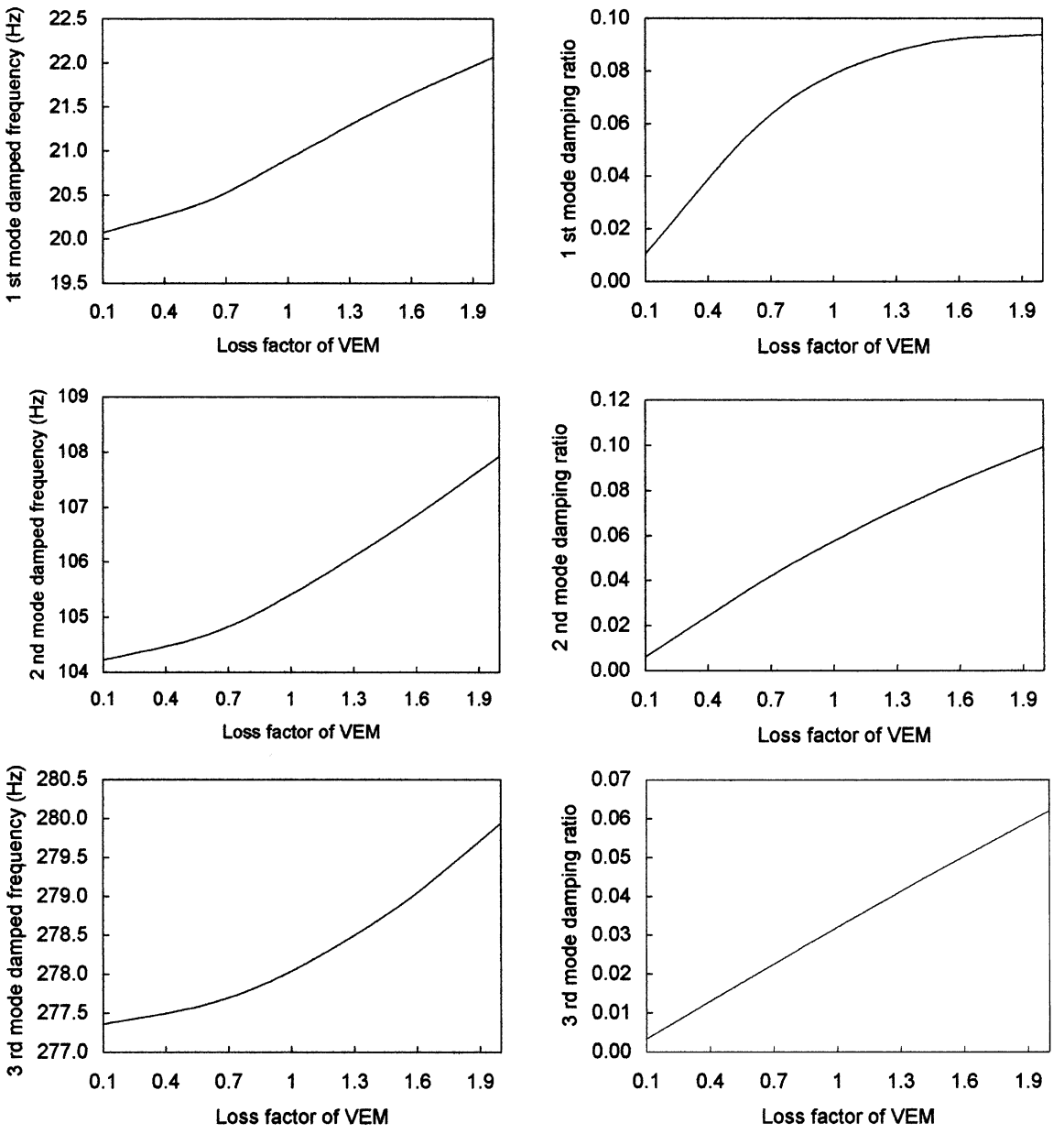

Fig. 4. The effect of VEM loss factor η on the first three modes of damped frequency and damping ratio for the case of PCLD ($K_p, K_d = 0$) when $\dot{\theta} = 200$ r.p.m. and $h_2 = 0.1094\ h_3$.

vibration of the system is intensified (Fig. 2). When the thickness ratio h_2/h_3 is increased, the damping of the system will be increased and the damped frequency of the system will be reduced. However, there is no appreciable improvement in the damping ratio (Fig. 3). Fig. 4 shows that although the damped frequency increases with an increase in the loss factor η of VEM, there is

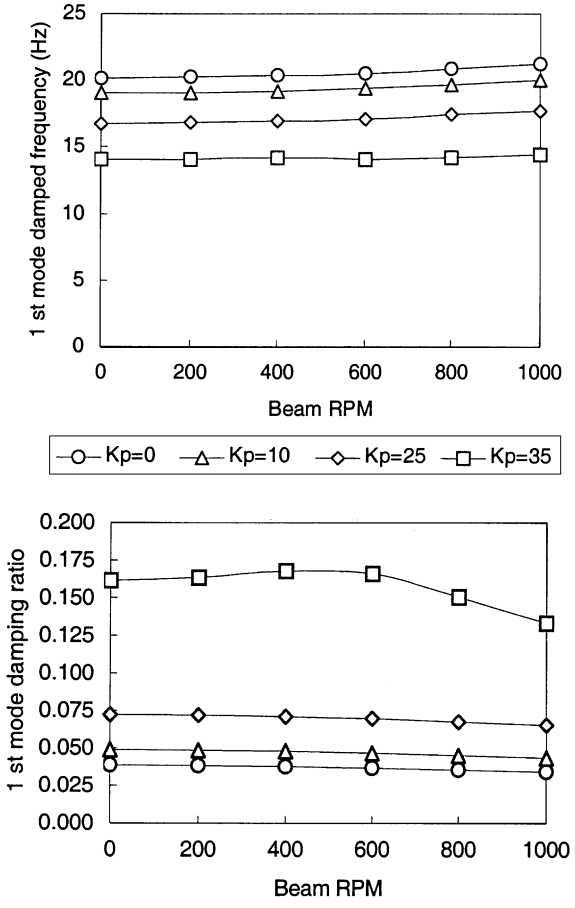

Fig. 5. The effect of angular velocity $\dot{\theta}$ on the first mode damped frequency and damping ratio for ACLD beam under different values of K_p when $h_2 = 0.1094h_3$ and $\eta = 0.38$.

substantial increase in the damping ratio with an increase of η which means that the vibration of the system is greatly suppressed.

For the case of ACLD, Fig. 5 shows the effect of the variation of rotating speed $\dot{\theta}$ on the first mode damped frequency and damping ratio under different values of proportional control gain K_p. It can be seen that increasing the proportional control gain K_p will reduce the first mode damping frequency and will increase the damping ratio. The maximum value that K_p can be increased is around 35. When K_p is increased beyond this value, instability of numerical results occurs. Fig. 6 shows the variation of the thickness ratio h_2/h_3 on the first mode damped frequency and damping ratio under different values of proportional control gain K_p. The first mode damped frequency and damping ratio are found to decrease and increase, respectively, with an increase in K_p. This effect is more obvious at high h_2/h_3 (i.e. $h_2/h_3 = 1.4$). Unlike the case of Fig. 5 the maximum value of K_p is around 12. Fig. 7 shows the variation of the VEM loss factor η on the first mode damped frequency and damping ratio under different values of proportional control gain K_p. Similar to the case of Figs. 5 and 6, the first mode damped frequency and damping ratio

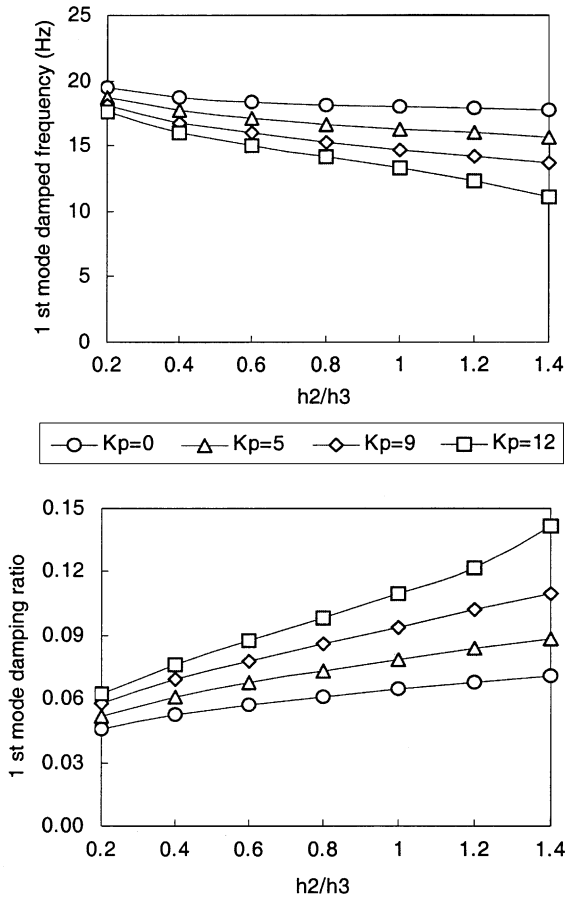

Fig. 6. The effect of thickness ratio h_2/h_3 on the first mode damped frequency and damping ratio for ACLD beam under different values of K_p when $\dot{\theta} = 200$ r.p.m. and $\eta = 0.38$.

are found to decrease and increase, respectively, with an increase in K_p and the effect on the damping ratio is intensified at high η (i.e. $\eta = 2.0$). The maximum value of K_p for stable numerical results in this case is around 30.

Although Figs. 5–7 show results on the first mode only, similar results are expected for the second and third modes. The results show that the proportional control can be used to attenuate the induced vibrations of the system. The effect of derivative control gain K_d on the vibration characteristic of the system will be considered in future study.

6. Conclusions

This paper has investigated the vibration behavior and control of a clamped–free rotating flexible cantilever arm rotating in a horizontal plane with fully covered active constrained layer damping (ACLD) treatment. The stress–strain relationship for the viscoelastic material (VEM) is described by a complex shear modulus. Hamilton's principle in conjunction with finite element

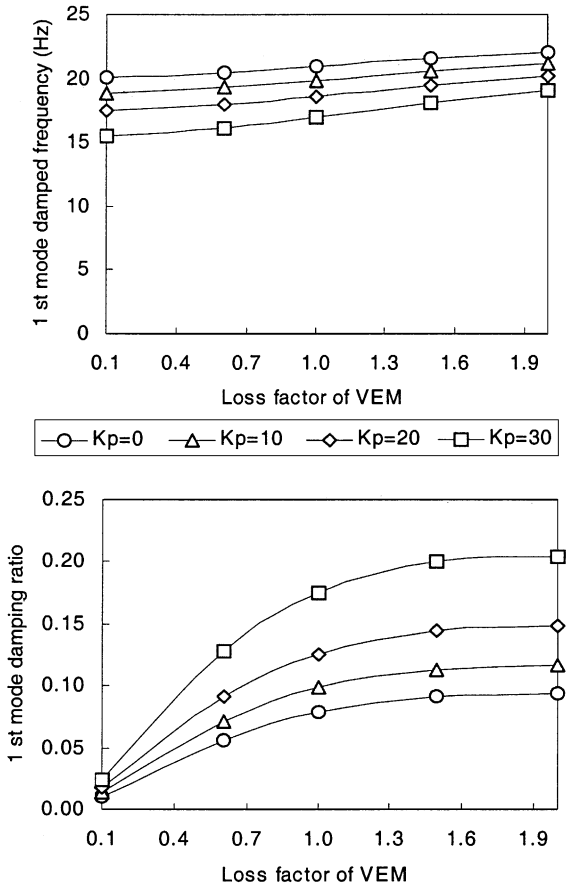

Fig. 7. The effect of VEM loss factor η on the first mode damped frequency and damping ratio for ACLD beam under different values of K_p when $\dot{\theta} = 200$ r.p.m. and $h_2 = 0.1094\ h_3$.

method (FEM) is used to derive the governing equations of motion. PD controllers are designed for the piezosensor and actuator. The closed-loop equation of motion for the system is derived and the characteristic complex eigenvalue problem is solved numerically. The effects of different rotating speed, thickness ratio and loss factor of the VEM as well as different controller gain on the damped frequency and damping ratio are presented. The results show that the proportional control gain K_p is effective in attenuating the induced vibration of this system. Further study will include the effects of derivative control gain K_d on the system. The results of this study will be useful in the design of adaptive and smart structures for vibration suppression and control in rotating structures such as rotorcraft blades or robotic arms.

Acknowledgements

The authors would like to thank The Hong Kong Polytechnic University Research Grant Committee for financial support (Project No. G-YC94) towards this work.

Appendix A. Nomenclature

A sensor surface area
A_k cross-sectional area of the kth layer ($= bh_k$)
b beam width
C capacitance of sensor
d_{31} piezoelectric strain constant
D_d distance from beam neutral axis to sensor surface
E_1I_1 flexural rigidity of piezoactuator
E_2I_2 flexural rigidity of viscoelastic core
E_3I_3 flexural rigidity of beam/sensor layer
$f(x)$ distribution shape function of sensor
G_2 complex shear modulus of viscoelastic core ($= G_2'(1 + \mathrm{i}\eta)$)
G_2' storage shear modulus of viscoelastic core
g_{31} piezoelectric voltage constant
h_1 thickness of piezoactuator
h_2 thickness of viscoelastic core
h_3 thickness of piezosensor/beam
i $\sqrt{-1}$
J moment of inertia of the hub
$K_{d,p}$ derivative and proportional control gains
k_{31} electro-mechanical coupling factor
k_{3t} dielectric constant
L length of beam
L_i length of beam element
m mass per unit width and unit length of the sandwiched beam ($= \rho_1h_1 + \rho_2h_2 + \rho_3h_3$)
q external transverse loads per unit width and unit length of the sandwiched beam
t time
T kinetic energy
U potential (strain) energy
u_1 longitudinal deflection of neutral axes of piezoactuator
u_2 longitudinal deflection of neutral axes of viscoelastic core
u_3 longitudinal deflection of neutral axes of piezosensor/beam layer
$v(t)$ piezoactuator voltage
V_s piezosensor voltage
W work done
w transverse deflection of the beam system
x position along beam
ρ_k density of the kth layer
γ shear strain of viscoelastic core
$\dot{\theta}$ angular velocity of flexible beam
λ_j jth closed-loop eigenvalue
σ_j real part of jth eigenvalue
τ applied hub torque

η loss factor of viscoelastic core
ω_j jth mode damped frequency

References

[1] M.A. Trindade, A. Benjeddou, R. Ohayon, Modeling of frequency-dependent viscoelastic materials for active-passive vibration damping, American Society of Mechanical Engineers, Journal of Vibration and Acoustics 122 (2000) 169–174.
[2] R.M. Christensen, Theory of Viscoelasticity: An Introduction, Academic Press, New York, 1971.
[3] R.L. Bagley, R.A. Calico, Fractional order state equations for the control of viscoelastically damped structures, Journal of Guidance, Control, and Dynamics 14 (1991) 304–311.
[4] D.J. McTavish, P.C. Hughes, Modeling of linear viscoelastic space structures, American Society of Mechanical Engineers, Journal of Vibration and Acoustics 115 (1993) 103–110.
[5] G.A. Lesieutre, E. Bianchini, Time domain modeling of linear viscoelasticity using anelastic displacement fields, American Society of Mechanical Engineers, Journal of Vibration and Acoustics 117 (1995) 424–430.
[6] C.D. Johnson, D.A. Kienholz, Finite element prediction of damping in structures with constrained viscoelastic layers, American Institute of Aeronautics and Astronautics Journal 20 (1982) 1284–1290.
[7] V.V. Varadan, Y.H. Lim, V.K. Varadan, Closed loop finite-element modeling of active/passive damping in structural vibration control, Smart Materials and Structures 5 (1996) 685–694.
[8] D.K. Rao, Frequency and loss factors of sandwich beams under various boundary conditions, Journal of Mechanical Engineering Science 20 (1978) 271–282.
[9] A. Baz, J. Ro, Vibration control of rotating beams with active constrained layer damping, Smart Materials and Structures 10 (2001) 112–120.
[10] A. Baz, Dynamic boundary control of beams using active constrained layer damping, Mechanical Systems and Signal Processing 11 (1997) 811–825.
[11] A. Baz, J. Ro, Performance characteristics of active constrained layer damping, Shock and Vibration 2 (1995) 33–42.
[12] Y.M. Shi, Z.F. Li, H.X. Hua, Z.F. Fu, The modelling and vibration control of beams with active constrained layer damping, Journal of Sound and Vibration 245 (2001) 785–800.
[13] V. Balamurugan, S. Narayanan, Finite element formulation and active vibration control study on beams using smart constrained layer damping (SCLD) treatment, Journal of Sound and Vibration 249 (2002) 227–250.
[14] U. Lee, J. Kim, Spectral element modeling for the beams treated with active constrained layer damping, International Journal of Solids and Structures 38 (2001) 5679–5702.
[15] Z. Wang, S. Chen, W. Han, Integrated structural and control optimization of intelligent structures, Engineering Structures 21 (1999) 183–191.
[16] R.D. Cook, Concepts and Applications of Finite Element Analysis, Wiley, New York, 2002.
[17] L. Meirovitch, Dynamics and Control of Structures, Wiley, New York, 1990.
[18] M.K. Kwak, New admissible functions for the dynamic analysis of a slewing flexible beam, Journal of Sound and Vibration 210 (1998) 581–592.
[19] H.H. Yoo, S.H. Shin, Vibration analysis of rotating cantilever beams, Journal of Sound and Vibration 212 (1998) 807–828.
[20] Y.A. Khulief, Vibration suppression in rotating beams using active modal control, Journal of Sound and Vibration 242 (2001) 681–699.
[21] L. Meirovitch, A new method of solution of the eigenvalue problem for gyroscopic systems, American Institute of Aeronautics and Astronautics Journal 12 (1974) 1337–1342.
[22] L. Zhang, J.W. Zu, Z. Hou, Complex modal analysis of non-self-adjoint hybrid serpentine belt drive systems, American Society of Mechanical Engineers, Journal of Vibration and Acoustics 123 (2001) 150–156.
[23] E.H.K. Fung, D.T.W. Yau, Effects of centrifugal stiffening on the vibration frequencies of a constrained flexible arm, Journal of Sound and Vibration 224 (1999) 809–841.